Alfvénic Instabilities and Fast Ion Transport in the DIII-D Tokamak

M.A. Van Zeeland 1), W.W. Heidbrink 2), R. Nazikian 3), M.E. Austin 4), H.L. Berk 4), N.N. Gorelenkov 3), C.T. Holcomb 5), G.J. Kramer 3), J. Lohr 1), Y. Luo 2), M.A. Makowski 5), G.R. McKee 6), C.C. Petty 1), R. Prater 1), W.M. Solomon 3), R.B. White 3)

1) General Atomics, P.O. Box 85608, San Diego, California 92186-5608, USA
2) University of California-Irvine, Irvine, California, USA
3) Princeton Plasma Physics Laboratory, Princeton, New Jersey, USA
4) University of Texas-Austin, Austin, Texas, USA
5) Lawrence Livermore National Laboratory, Livermore, California, USA
6) University of Wisconsin-Madison, Madison, Wisconsin, USA

e-mail contact of main author: vanzeeland@fusion.gat.com

Abstract. Neutral beam injection into reversed magnetic shear DIII-D plasmas produces a variety of Alfvénic activity including Toroidicity and Ellipticity induced Alfvén Eigenmodes (TAE/EAE, respectively) and Reversed Shear Alfvén Eigenmodes (RSAE) as well as their spatial coupling. These modes are typically studied during the discharge current ramp phase when incomplete current penetration results in a high central safety factor and strong drive due to multiple higher order resonances. During this same time period Fast-Ion D_α (FIDA) spectroscopy shows that the central fast ion profile is flattened, the degree of which depends on the Alfvén eigenmode amplitude. Interestingly, localized electron cyclotron heating (ECH) near the mode location stabilizes RSAE activity and results in significantly improved fast ion confinement relative to discharges with ECH deposition on axis. In these discharges, RSAE activity is suppressed when ECH is deposited near the radius of the shear reversal point and enhanced with deposition near the axis. To simulate the observed neutral beam ion redistribution, NOVA calculations of the 3D eigenmode structures are matched with experimental measurements and used in combination with the ORBIT guiding center following code. For fixed frequency eigenmodes, it is found that ORBIT calculations cannot explain the observed beam ion transport with experimentally measured mode amplitudes. Possible explanations are considered including recent simulation results incorporating eigenmodes with time dependent frequencies.

1. Introduction

Future burning plasma experiments such as ITER may be subject to the excitation of Alfvén eigenmode (AE) instabilities by 3.5 MeV fusion born alpha particles needed to sustain the thermonuclear burn as well as neutral beam ions critical for current drive, heating, and momentum input [1,2]. If allowed to grow unabated, these instabilities have the potential to cause fast ion redistribution or loss and possible damage to first wall components. Consequently, developing validated predictive models for this nonlinear interaction as well as control techniques to suppress these instabilities is critical for extrapolating to ITER and beyond.

Recent experimental results from the DIII-D tokamak have validated several key elements of AE theory including the linear coupling of multiple AEs [3], excitation of AEs by sub-Alfvénic beam ions via higher order resonances [4], and spatial eigenmode structure of various AEs in reversed magnetic shear plasmas [3,5]. These studies have also yielded several surprising findings. First, localized electron cyclotron heating (ECH) near the mode location stabilized reversed shear Alfvén eigenmodes (RSAEs) [6] and results in significantly improved fast ion confinement relative to similar discharges with ECH deposition on axis [7]. Second, detailed orbit-following simulations using multiple experimentally validated eigenmodes fail to reproduce the large measured fast ion deficit [8,9].

This paper begins with an explanation of the discharge parameters and Alfvén eigenmodes present, as well as modeling of AE mode structure and spectral evolution. In the next several sections, a description of the observed fast ion transport is given followed by a summary of recent experiments studying the effect of ECH on RSAE activity and the

consequent reduction of fast ion transport. In the last section, modeling of the interaction of AEs with fast ions is discussed and simulations of the transport are presented.

2. Experiment and Modeling – AE Spectral Evolution and Eigenfunctions

The primary discharge of interest in this study is analyzed during the current ramp phase [Fig. 1(b)] when 5 MW, 78 kV, unbalanced co-going, sub-Alfvénic ($V_B/V_A \sim 0.4$), neutral deuterium beams are injected into the plasma. The central β (plasma pressure/magnetic field pressure) is increasing during this period, and there is an off-axis minimum in the magnetic safety factor ($q_{\min}$). The electron density is relatively low $\sim 2\times10^{19}$ m^{-3}, and the fast-ion pressure is roughly half of the total plasma pressure according to TRANSP [10] analysis. Several fluctuation diagnostics indicate a variety of Alfvénic activity in this discharge. Shown in Fig. 1(a) is a crosspower spectrum of a beam emission spectroscopy (BES) channel located near $q_{\min}$ and a vertical CO2 interferometer chord. Previous analysis has identified the modes chirping up in frequency as RSAEs and the series of relatively constant frequency modes as TAEs [3,5] (for reference, the TAE frequency at $q_{\min}$ is plotted in Fig. 1(c) as well as the charge exchange recombination measured toroidal rotation frequency at $q_{\min}$). Over the time window shown, the RSAE spectral behavior is typical for decreasing $q_{\min}$ with an integer crossing ($q_{\min} = 4$) at approximately $t = 410$ ms [5,11]. Plotted in Fig. 1(b) (solid-diamonds) are values of $q_{\min}$ derived from the RSAE activity [11] in combination with motional Stark effect (MSE) measurements [12].

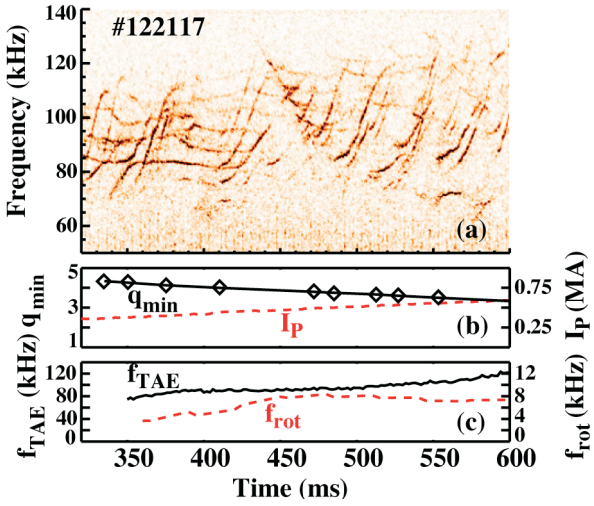

FIG. 1. Data from DIII-D discharge 122117. (a) power spectrum of a vertical CO2 interferometer chord and BES channel near $q_{\min}$. (b) $q_{\min}$ evolution inferred from RSAEs (diamonds) and MSE (solid), plasma current (dashed). (c) TAE frequency (solid) and toroidal rotation frequency (dashed) at $q_{\min}$.

Precise knowledge of the $q_{\min}$ evolution made possible through RSAE identification is fundamental to the recently reported progress in AE modeling using the NOVA code [5,13,14]. An example of the NOVA calculated eigenfrequencies for a subset of Fig. 1(a) is shown in Fig. 2(b), where n = 2–4 RSAEs and two $n = 3$ TAEs are identified and excellent agreement with the experimentally measured spectral evolution [Fig. 2(a)] is shown. The occasional gaps in the experimentally observed mode amplitudes and frequency evolution, such as that appearing at approximately t = 352 ms, f = 83 kHz are a signature of mode-mode coupling and have been investigated in detail recently [3]. It was found this particular gap was formed by the coupling of an $n = 3$ RSAE and $n = 3$ global TAE, behavior which is reproduced by the NOVA modeling near $q_{\min}$ = 4.23. Throughout the coupling process, the calculated spatial

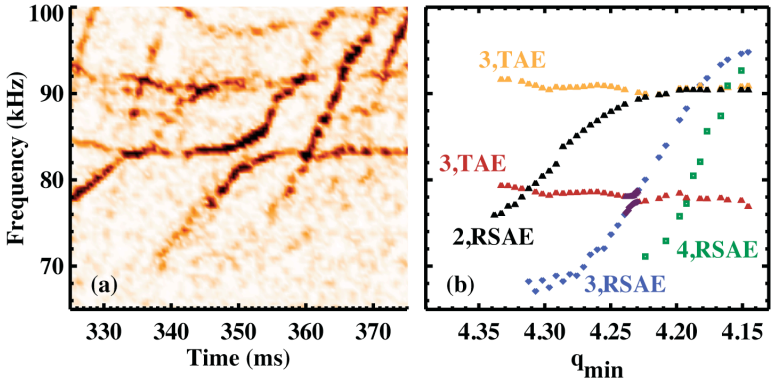

FIG. 2. (a) Enlarged region of Fig. 1(a). (b) NOVA modeling for $q_{\min}$ range of panel (a) showing calculated frequencies for several RSAEs and TAEs. Modes are identified with toroidal mode number followed by type of eigenmode.

eigenmodes are linear odd/even parity combinations of the two original eigenmodes, a process that has been verified in detail by comparison with electron cyclotron emission (ECE) measurements [3].

A comparison of the NOVA calculated eigenmode with ECE data is shown in Fig. 3(a) for the $f \sim 78$ kHz $n = 3$ TAE from Fig. 2(b). For comparison with ECE measurements, a synthetic diagnostic as described in Ref. [5] is used to process the NOVA predicted temperature perturbation. By scaling the NOVA prediction by a single constant to match the ECE data the amplitude of the perturbation wavefields is obtained. The inferred amplitude is shown in Fig. 3(c) where the radial magnetic field perturbation (δB_r) is scaled to the local magnetic field strength $|B|$. This perturbed field amplitude combined with the poloidal harmonic structure [Fig. 3(b)] forms the input for the fast ion transport modeling that will be discussed in section 5.

3. Fast Ion Transport and TRANSP Modeling

Data from several fast ion diagnostics indicate that during periods of strong Alfvénic activity the central fast ion population is significantly depleted relative to expectations based on neoclassical diffusion alone [8,9]. The measurements involved in this finding are Fast Ion D_α spectroscopy (FIDA) [15], volume-averaged neutron emission, and EFIT [16] magnetic equilibrium reconstructions, which use MSE diagnostic data as a constraint to obtain the internal pressure profile. An example of the observed fast ion profile flattening is shown in Fig. 4(a) where the fast ion pressure profile inferred from equilibrium reconstructions is given along with FIDA measurements and the classical TRANSP prediction [8,9]. The fast ion pressure is obtained from equilibrium reconstructions by subtraction of the measured thermal pressure. These data correspond to t = 365 ms in Fig. 1 and Fig. 2(a). Throughout the same time range the neutron rate is approximately 50% of that predicted by TRANSP. Due to the fact that in these discharges, the primary neutron sources are beam-plasma and beam-beam fusion reactions, this is also consistent with a large radial transport of the beam ions. The FIDA measured profile modification can be quantified in an approximate way by the gradient of a straight line fit to the radial profiles — more transport results in a flattened profile and reduced gradient. In the first study of its kind, a large database of fast ion profile measurements drawing from DIII-D discharges in the 2006 and 2007 run campaigns was created [9]. Collectively, these data show a strong correlation between fast ion redistribution and Alfvén eigenmode amplitude.

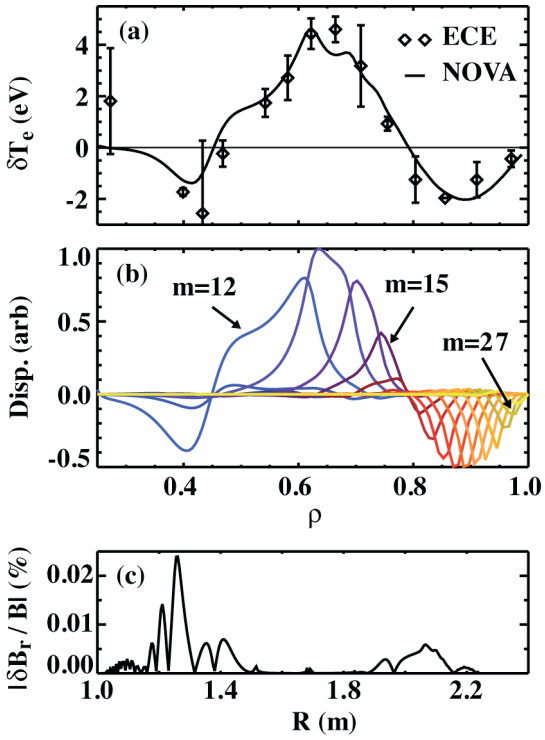

FIG. 3. (a) Synthetic ECE diagnostic prediction (solid) using NOVA calculated f = 78 kHz $n = 3$ global TAE from Fig. 2 overlayed with ECE measurements (diamonds). NOVA prediction scaled by single constant to match ECE data. (b) Poloidal harmonics comprising TAE from panel (a). (c) Calculated radial component of magnetic field fluctuation along device midplane using amplitude obtained from comparison with ECE data.

In order to model these discharges, and estimate the experimental transport, a range of ad hoc fast ion diffusion coefficients D_B was employed in a sequence of TRANSP runs and the resultant predictions for neutron emission and fast ion pressure are compared with

experimental data [9]. TRANSP allows a radially varying diffusivity profile [$D_B(\rho)$], which is important for obtaining results that are consistent with experimental measurements.

TRANSP modeling for three specified diffusivity profiles are shown in Fig. 4(b), where the $D_B(\rho)$ profiles are given in the inset. The three cases correspond to: no diffusion, constant $D_B(\rho) = 1.5\ \mathrm{m}^2/\mathrm{s}$, and radially varying $D_B(\rho < 0.5) = 5\ \mathrm{m}^2/\mathrm{s}$. The no diffusion case is unable to reproduce experimental measurements as discussed above, but both finite diffusivity cases reproduce the experimental neutron measurements within the estimated errors. The two results differ in the predicted fast ion pressure profiles shown [Fig. 4(b)], where the constant diffusion profile prediction is seen to remain centrally peaked while the high inner diffusivity case causes significant flattening [9]. While it is true that the $D_B(\rho)$ profile cannot be not uniquely determined in this manner, a large central diffusion with classical levels outside mid-radius is most consistent with experimental data during strong AE activity, a fact which is confirmed by several other studies that model the $q_{\min}$ evolution [9] and momentum diffusivities [17].

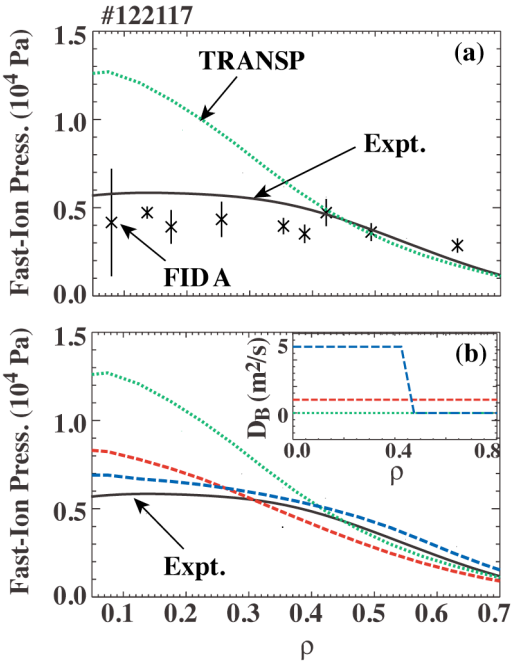

FIG. 4. (a) Experimental (solid) and TRANSP modeled (dotted) fast ion pressure profile in discharge 122117 at t = 365 ms. Experimental fast ion pressure profile is obtained from EFIT reconstructions subtracting off the measured thermal pressure from the total pressure. Data points are FIDA measurements. (b) TRANSP estimates for fast ion pressure with three separate diffusivity profiles shown in inset.

4. ECH Stabilization of RSAEs and Impact on Fast Ion Transport

Interestingly, the use of ECH in a set of experiments designed to probe the RSAE dependence on finite pressure effects resulted in the almost complete stabilization of RSAEs and a significant effect on the observed fast ion transport [7]. The discharge used in this experiment was very similar to #122117 discussed in the previous sections. The major difference is that during the current rise phase, approximately 1.9 MW of 110 GHz ECH power was injected radially to heat electrons and minimize net current drive. Both ECH and NBI injection begin at t=300 ms and remain on throughout the current ramp phase. A typical equilibrium magnetic flux surface reconstruction overlayed with two of the ray trajectories used in the experiment is shown in Fig. 5(a). The ray trajectories do not include refraction so the actual deposition location at the second electron cyclotron harmonic layer ($2fc_e$) was at slightly larger minor radius. The trajectory marked *II* terminates near the shear reversal point ($\rho_{q\min}$) and that marked *I* is closer to the magnetic axis.

The suppression of RSAE activity when ECH is deposited near $\rho_{q\min}$ is shown in Fig. 5(b,c), where crosspower spectra of vertical and radial CO2 interferometer chords is shown. Each of these spectra show a variety of Alfvén eigenmodes typical for this type of discharge and similar to that shown for discharge 122117 in Fig. 1. The primary difference between these discharges is the dramatic lack of RSAE activity for ECH deposition near $q_{\min}$ [Fig. 5(c)]. In Fig. 5(c) only the very end of RSAE chirps are visible where the RSAEs transition to TAEs. The combined local TAE frequency and toroidal rotation frequency near $q_{\min}$ ($f_{\mathrm{TAE}} + f_{rot}$) is overlayed as well as a typical RSAE frequency sweep highlighted in Fig. 5(b). The overplotted ($f_{\mathrm{TAE}} + f_{rot}$) represents the approximate frequency of an $n = 1$ TAE near $q_{\min}$. The majority of the TAEs shown are $n > 1$ and will be Doppler shifted to larger frequencies given approximately by $f_{\mathrm{TAE}} + nf_{rot}$. The modes sweeping up in

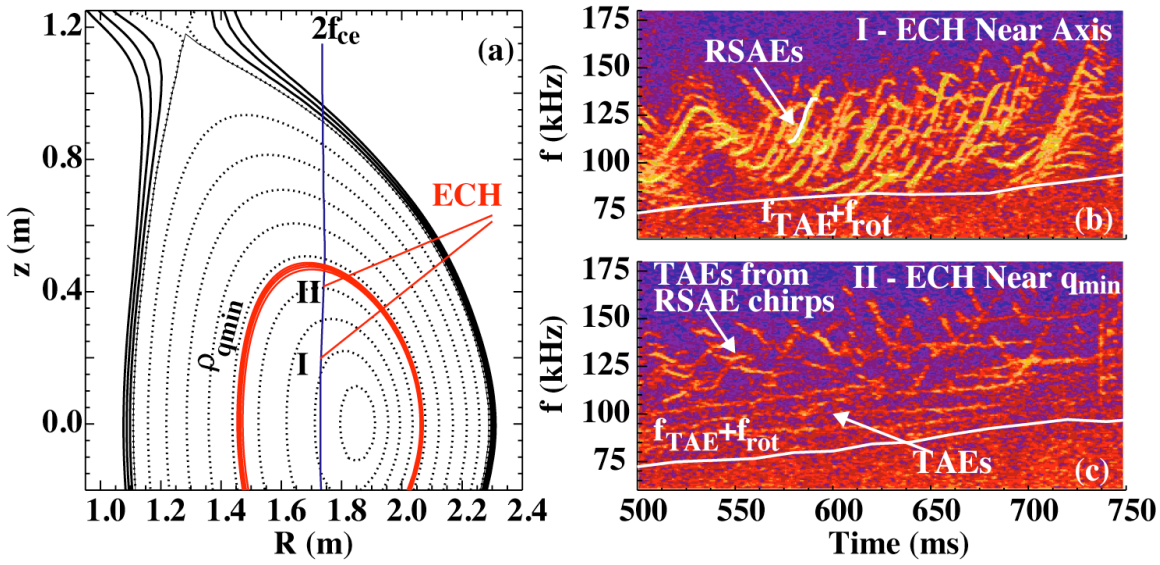

FIG. 5. (a) Representative equilibrium overlayed with ECH ray trajectories for heating near q_{min} (II) and near the axis (I). (b) Crosspower spectrum of vertical and radial interferometer showing RSAE activity during ECH deposition near axis. Typical RSAE frequency evolution highlighted at t~550 ms. (c) Spectrum showing lack of RSAE activity during ECH deposition near q_{min}. Same color scale is used for (b) and (c).

frequency on the timescale of 10–20 ms are RSAEs and the relatively constant frequency modes are global TAEs or the TAEs resulting from the RSAE to TAE transition. Other low level TAEs have emerged for the case of ECH deposition near q_{min} and are seen as a series of modes with slowly varying frequencies in the range just above the overplotted TAE frequency [7].

There is evidence for improved beam ion confinement in the discharges with ECH deposition near q_{min} and stabilized RSAEs. As a measure of the level of Alfvénic activity, Fig. 6(a) shows the temporal evolution of the integrated power in the TAE/RSAE range (50–230 kHz) of the CO2 interferometer data presented in Fig. 5. Figure 6(b) shows the relative impact on volume averaged neutron production compared to TRANSP simulations. The discharge with ECH deposition near q_{min} and stabilized RSAE activity has higher S_n relative to the discharge with significant RSAE activity. This increased neutron emission when scaled to TRANSP predictions can only be due to reduced fast ion transport. An interesting point however, is that up to 60% of the S_n reduction remains, indicating that the bulk of the neutron deficit is not due to RSAE activity in these discharges.

Further evidence of improved fast ion confinement, is given in Fig. 6(c), which shows fast ion D_α (FIDA) measurements of the density of high-energy beam ions (n_{FI}) near the magnetic axis. Similar to the neutron measurements, n_{FI} is smallest for ECH deposition near the axis. In terms of fast ion density, this is in contrast to what one

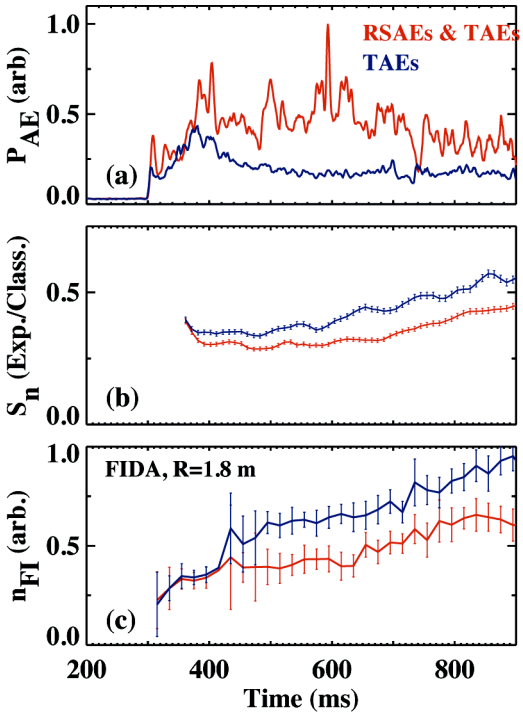

FIG. 6. (a) Bandpass filtered (50–230 kHz) crosspower spectrum from Fig. 5 for deposition near magnetic axis (red) and near q_{min} (blue) – a measure of AE amplitude. (b) Volume averaged neutron emission scaled to TRANSP predictions. (c) Central fast ion density measured by FIDA.

would expect based purely on neutral beam ions slowing down classically due to electron drag. With the higher central T_e for ECH deposition near the axis, one would expect larger fast ion density on-axis. This is clearly not the case and the increased fast ion density on-axis for ECH deposition near $q_{\min}$ is attributed to reduced fast ion radial transport in the discharges with little or no RSAE. Before $t \approx 400$ ms, when the overall level of Alfvénic activity is similar, so is the measured fast ion density [7].

Currently, the actual RSAE stabilization mechanism is not known. Several possibilities have been investigated including the ECH enhancement of trapped electrons, current profile modification, current drive, and finite pressure effects on the mode minimum frequency. Qualitatively, the authors suggest that some combination of effects may be important. One possibility is that the RSAE is pushed into the continuum with increased rotation and pressure and the mode experiences increased continuum damping. Such an interaction could be sustained by increased central rotation and large rotation shear resulting from reduced fast ion transport which will further push the RSAE into the continuum. Other complicating factors in understanding this process include a significant change to the slowing down time and fast ion distribution itself, thus changing the mode drive.

5. Modeling the Interaction of AEs and Fast Ions

In a first step toward understanding the interaction of the observed Alfvén eigenmodes with the fast ion population, a linear stability analysis is carried out using the NOVA-K code [18,19]. This code uses the ideal MHD eigenmode solutions generated by NOVA and calculates the drive and damping using a perturbative procedure incorporating the fast ion distribution through an analytic approximation to TRANSP analysis. Figure 7(a) displays a plot of the analytical beam ion distribution generated for beam ions in the plasma of Fig. 1 at t = 359 ms. The overplotted solid lines represent boundaries for different classes of orbits. The color surface plot represents beam ion density at one-half the injection energy plotted vs. normalized fast ion invariants of the motion, $\lambda = \chi^2 R/R_0$ and P_ζ/ψ_W, where $\chi = V_\perp/V_b$, $P_\zeta = V_\parallel B_0/B - \psi_{pol}(r)$ is the canonical momentum, $\psi_{pol}(r)$ is the poloidal magnetic flux at minor radius r, ψ_W is the poloidal flux at the last closed flux surface, B is the local magnetic field strength, B_0 is the magnetic field strength on the magnetic axis [4]. In Fig. 7(a) the majority of beam ions are deposited in a relatively small region of velocity space that is comprised primarily of co-passing particles. Physically, the axes can be explained as follows. Moving up the vertical axis, the pitch angle of the particle relative to the magnetic field line increases so particles are deeply passing at low values of the vertical axis and deeply trapped at the upper range. Along the horizontal axis, particles are moving in the direction counter to the plasma current to the far left and move in the direction of the plasma current toward the right, with an offset determined by the magnetic flux at the particle location [4].

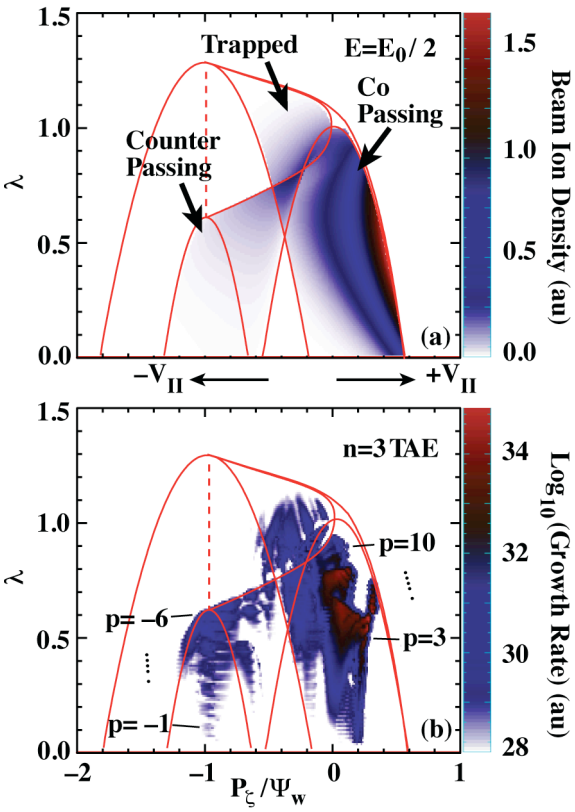

FIG. 7. (a) Analytic model based on TRANSP results for 40 keV ion distribution function in 122117 at t = 359 ms. Solid red curves represent boundaries for different classes of orbits [4]. (b) NOVA-K calculated drive integrated over all energies for $n = 3$ TAE of Fig. 3. Range of resonance orders (p) labeled.

Figure 7(b) shows the calculated drive integrated over all energies for the $n = 3$ TAE of Fig. 3. From this plot it is immediately clear that a large fraction of the fast ion population can contribute to the drive for this mode. The boundaries shown are approximate and only strictly correct for 40 keV, however, it can be seen that the dominant drive is coming from co-passing particles and perhaps surprisingly, some drive is coming from the counter passing particles. More precisely, this analysis identifies the role of higher order resonances in the mode excitation where the resonance order p is defined according to the standard passing particle resonance condition given by

$$\omega - n\omega_{pr} - \left[\left(m - nq\right) + p\right]\omega_{\theta} = 0 \quad ,$$

where ω_θ is the poloidal transit frequency, ω is the mode frequency, p is a nonzero positive or negative integer, and ω_{pr} is the particle toroidal precession frequency [4]. Physically, this equation is equivalent to the statement that when a resonant particle makes a full transit in the poloidal angle, the phase of the wave with poloidal/toroidal mode numbers m/n at the particle should change by a multiple of 2π [20]. Again, in interpreting Fig. 7(b), the initial particle distribution must be considered since it is convolved with the relative strength of each resonance. The relative strength of the drive for a given p is a strong function of the discharge equilibrium. The fundamental $p = \pm 1$ resonance represents the strongest channel for wave particle interaction, when $m\rho_{fi}/r << 1$; however, at high $q_{\min}$ as in these discharges, $m\rho_{fi}/r \geq 1$, where ρ_{fi} is the fast ion gyroradius and r is the minor radius. High $q(0)$ reversed shear plasmas such as these lead to significant higher order resonant drive since the particle poloidal trajectory exhibits large deviations from flux surfaces, particularly near the magnetic axis where the poloidal field is relatively small [4,21]. Mathematically, the poloidal drift motion can be expanded in Fourier harmonics of the poloidal angle and the Fourier amplitude of a given harmonic is directly related to the higher order resonance drive. This dominance of higher order resonances is something that must be considered in reversed magnetic shear plasmas such as those in advanced tokamak plasmas as well as in burning plasmas where high-n instabilities are expected.

The NOVA-K calculations indicate that resonant energy transfer can occur throughout a significant fraction of the fast ion distribution. The primary numerical tool used to assess fast ion transport is ORBIT [22], a Hamiltonian guiding center code in combination with NOVA calculated eigenmodes. This is carried out by taking the 11 largest amplitude modes, and matching the NOVA linear eigenfunctions with ECE measurements. The amplitudes are obtained by scaling the predicted temperature perturbation to match that of the ECE data as presented in Fig. 3. In total 151 different poloidal harmonics with their experimental amplitudes and frequencies are entered into ORBIT [8,9]. The particle trajectories are then followed in the presence of the wavefields as well as pitch angle scattering due to collisions. In these simulations, evolution of the frequency and mode structure is ignored but will be mentioned briefly at the end of the section. The initial fast-ion birth distribution function F_0 is that from Fig. 7(a) as calculated by TRANSP. The evolving distribution function F is recorded at several timesteps for comparison with F_0.

The impact of the modes on the fast ion population is found by integrating F over energy and pitch in the desired region to obtain a fast ion density with collisions (n_{FI}) and with collisions plus modes ($n_{\mathrm{FI\text{-}modes}}$). The difference between these is a measure of the modes' ability to cause fast ion transport. The net result of this ORBIT modeling is that even with five times the measured mode amplitudes, the large experimentally observed fast ion transport cannot be explained [8,9].

Several possible explanations for this discrepancy are considered in detail in reference [9]. One distinct possibility is the presence of other modes that have previously gone undetected. A strong candidate for this is the recently discovered BAAE that is often obscured by broadband turbulence in diagnostic signals. Another possibility is that the broadband turbulence itself is responsible [23].

Recently, ORBIT simulations have been carried out using model Gaussian shaped eigenmodes representative of those in experiment, but with time dependent eigenmode frequencies to simulate the realistic experimental conditions. This effect significantly increases the simulated transport. Although a preliminary result, the primary cause for this enhanced transport is that by allowing time varying frequencies, a single mode is able to affectively interact with many more particles in the distribution function.

6. Conclusions

Significant progress has been made recently in understanding several aspects of Alfvén eigenmodes in reversed magnetic shear DIII-D plasmas, including eigenmode structure, mode coupling, and the higher order resonance drive responsible for mode growth. Surprisingly, progress was even made toward control of these instabilities when it was empirically observed that ECH, when applied near the shear reversal point, could be used to effectively target and stabilize RSAEs with a significant impact on fast ion confinement. However, a complete understanding is not yet at hand in that these modes are observed to be correlated with a large redistribution of energetic ions that ORBIT simulations using measured modes fail to explain. Recent work using the experimental mode frequency evolution appears to be encouraging and will be presented in an upcoming publication; however, every step toward a more realistic formulation of the problem highlights the inherent difficulty with this type of approach — the fact that the calculation is not being done self-consistently. Future work should include a self-consistent multimode simulation in which the eigenmodes of the thermal/fast ion plasma are included as well as their interaction with background turbulence.

Acknowledgments

This work supported by the U.S. Department of Energy under DE-FC02-04ER54698, SC-G903402, DE-AC02-76CH03073, DE-FG03-97ER54415, DE-AC52-07NA27344, and DE-FG02-89ER53296.

References

[1] FU, G.Y., and VAN DAM J.W. Phys. Fluids B **1**, 1949 (1989).
[2] WONG, K.L., et al., Phys. Rev. Lett. **93**, 085002 (2004).
[3] VAN ZEELAND, M.A., et al., Phys. Plasmas **14**, 056102-1 (2007).
[4] NAZIKIAN, R., et al., Phys. Plasmas **15**, 056107 (2008).
[5] VAN ZEELAND, M.A., et al., Phys. Rev. Lett. **97**, 135001-1 (2006).
[6] KUSAMA, Y. et al., Nucl. Fusion **38**, 1215 (1998).
[7] VAN ZEELAND, M.A., et al., Plasma Phys. Control. Fusion **50**, 035009 (2008).
[8] HEIDBRINK, W.W., et al., Phys. Rev. Lett. **99**, 245002-1 (2007).
[9] HEIDBRINK, W.W., et al., Nucl. Fusion **48**, 084001 (2008).
[10] BUDNY, R.V., Nucl. Fusion **34**, 1247 (1994).
[11] VAN ZEELAND, M.A., et al., Nucl. Fusion **46**, S880 (2006).
[12] HOLCOMB, C.T., et al., Rev. Sci. Instrum. **77**, 10E506 (2006).
[13] CHENG, C.Z., and CHANCE, M.S., J. Comput. Phys. **71**, 124 (1987).
[14] CHENG, C.Z., Phys. Rep. **211**, 1 (1992).
[15] HEIDBRINK, W.W., et al., Plasma Phys. Control. Fusion **49**, 1457 (2007).
[16] LAO, L.L., ST. JOHN, H.E., STAMBAUGH, R.D., KELLMAN, A.G., PFEIFFER, W., Nucl. Fusion **25**, 1611 (1985).
[17] SOLOMON, W.M., this conference.
[18] GORELENKOV, N.N., CHENG, C.Z., FU, G.Y., Phys. Plasmas **6**, 2802 (1999).
[19] GORELENKOV, N.N., BERK, H.L., BUDNY, R., Nucl. Fusion **45**, 226 (2005).
[20] TODO, Y., and SATO, T., Phys. Plasmas **5**, 1321 (1998).
[21] HEIDBRINK, W.W., Phys. Plasmas **15**, 055501 (2008).
[22] WHITE, R.B., and CHANCE, M.S., Phys. Fluids **27**, 2455 (1984).
[23] GUNTER, S.,et al., Nucl. Fusion **47**, 920 (2007).